Gazi Üniversitesi
Fen Bilimleri Dergisi
PART C: TASARIM VE TEKNOLOJİ

Gazi University
Journal of Science
PART C: DESIGN AND TECHNOLOGY

GU J Sci, Part C, 14(1): 418-433 (2026)

Design and Thermal Elastic Behavior of FGM Sandwich Plate with TPMS Core Layer

Adem Fatih ÖZALP[1*]

[1]*Yalova University, Faculty of Engineering, Mechanical Engineering Department, Yalova, Turkey*

Article Info

Research article
Received: 13/12/2025
Revision: 23/02/2026
Accepted: 04/03/2026

Keywords

Sandwich Plate
TPMS
FGM
Material Properties

Makale Bilgisi

Araştırma makalesi
Başvuru: 13/12/2025
Düzeltme: 23/02/2026
Kabul: 04/03/2026

Anahtar Kelimeler

Sandviç Plaka
TPMS
FDM
Malzeme Özellikleri

Graphical/Tabular Abstract (Grafik Özet)

This study investigates the thermo-elastic behavior of an FGM sandwich plate with a TPMS lattice core. The effects of temperature rise, material grading index, and TPMS volume fraction on effective membrane and bending elastic properties are analyzed for Primitive, Gyroid, and IWP architectures./ Bu çalışma, TPMS kafes çekirdeğe sahip FGM sandviç plakanın termo-elastik davranışını incelemektedir. Sıcaklık artışı, malzeme derecelendirme indeksi ve TPMS hacim oranının efektif membran ve eğilme elastisite özellikleri üzerindeki etkileri Primitive, Gyroid ve IWP geometrileri için analiz edilmiştir.

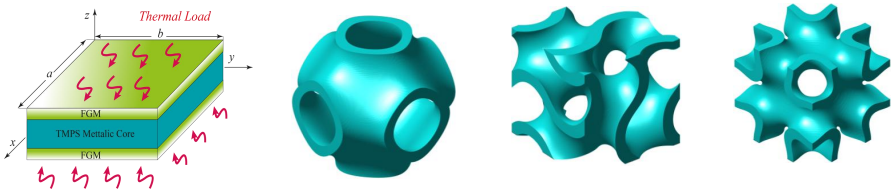

***Figure A**: Sandwich Plate and TPMS Structures /**Şekil A:**.Sandviç Plaka ve TPMS Yapıları*

Highlights (Önemli noktalar)

- *Thermo-elastic behavior of an FGM sandwich plate with TPMS lattice core is investigated. / TPMS kafes çekirdeğe sahip FGM sandviç plakanın termo-elastik davranışı incelenmiştir.*
- *Primitive, Gyroid and IWP TPMS architectures are analyzed / Primitive, Gyroid ve IWP TPMS geometrileri analiz edilmiştir.*
- *The influence of material grading index, temperature rise and TPMS volume fraction on effective mechanical properties is examined. / Malzeme derecelendirme indeksi, sıcaklık artışı ve TPMS hacim oranının efektif mekanik özellikler üzerindeki etkileri incelenmiştir.*
- *Membrane and bending elastic responses of the sandwich structure are evaluated. / Sandviç yapının membran ve eğilme elastik tepkileri incelenmiştir.*

***Aim (Amaç):** The aim of this study is to investigate the thermo-elastic behavior of a functionally graded sandwich plate with a TPMS lattice core by evaluating the influence of material grading index, temperature rise and TPMS volume fraction on the effective membrane and bending elastic properties of the structure. / Bu çalışmanın amacı, TPMS kafes çekirdeğe sahip fonksiyonel derecelendirilmiş bir sandviç plakanın termo-elastik davranışını incelemek ve malzeme derecelendirme indeksi, sıcaklık artışı ve TPMS hacim oranının yapının efektif membran ve eğilme elastisite özellikleri üzerindeki etkilerini değerlendirmektir.*

***Originality (Özgünlük):** A sandwich plate composed of TPMS lattice cores with functionally graded face sheets is evaluated for membrane and bending elastic responses for different TPMS architectures. / TPMS kafes çekirdek tabakası fonksiyonel derecelendirilmiş yüzey tabakalarından oluşan sandviç plakanın farklı TPMS geometrileri için membran ve eğilme elastik tepkileri değerlendirilmiştir.*

***Results (Bulgular):** Increasing temperature reduces both membrane and bending elastic moduli of the sandwich plate, while increasing the TPMS volume fraction enhances structural stiffness. The material grading index affects thermal expansion and mechanical stiffness, whereas thermal conductivity is mainly governed by the TPMS architecture and its volume fraction. / Sıcaklık artışının sandviç plakanın hem membran hem de eğilme elastisite modüllerini azalttığını, TPMS hacim oranının artmasının ise yapısal rijitliği artırdığı görülmüştür. Malzeme derecelendirme indeksi termal genleşme ve mekanik rijitliği etkilerken, ısıl iletkenlik daha çok TPMS geometrisi ve hacim oranı tarafından belirlenmektedir.*

***Conclusion (Sonuç):** The thermo-mechanical performance of FGM sandwich plates can be effectively controlled through the combined design of TPMS core, material gradation and temperature conditions. / FGM sandviç plakaların termo-mekanik performansının TPMS çekirdek geometrisi, malzeme derecelendirmesi ve sıcaklık koşullarının birlikte tasarlanmasıyla etkin şekilde kontrol edilebileceği görülmüştür.*

*Corresponding author, e-mail: ademfatih.ozalp@yalova.edu.tr
DOI: 10.29109/gujsc.1841430

GU J Sci, Part C, 14(1): 418-433 (2026)

Gazi Üniversitesi
Fen Bilimleri Dergisi
PART C: TASARIM VE TEKNOLOJİ

Gazi University
Journal of Science
PART C: DESIGN AND TECHNOLOGY

http://dergipark.gov.tr/gujsc

Design and Thermal Elastic Behavior of FGM Sandwich Plate with TPMS Core Layer

Adem Fatih ÖZALP[1*]

[1]*Yalova University, Faculty of Engineering, Mechanical Engineering Department, Yalova, Turkey*

Article Info

Research article
Received: 13/12/2025
Revision: 23/02/2026
Accepted: 04/03/2026

Keywords

Sandwich Plate
TPMS
FGM
Material Properties

Abstract

This study examines the thermo-mechanical behavior of a sandwich plate with functionally graded (FGM) face sheets and a TPMS (Triply Periodic Minimal Surface) core. The faces are made of Si_3N_4/SUS304 and follow a power-law distribution. The Primitive, Gyroid, and IWP TPMS structures are modeled through homogenized Gibson–Ashby relations. Temperature-dependent elastic and thermal properties are included for all layers. The analysis focuses on how the material grading index, temperature rise, and TPMS volume fraction change the equivalent in-plane elastic modulus and equivalent bending elastic modulus of the sandwich plate. In a homogeneous solid plate, the in-plane (membrane) and bending responses are uncoupled and governed by uniform stiffness through the thickness. In contrast, plates with a compliant core, such as sandwich structures, exhibit different effective membrane and bending elasticities due to the non-uniform stiffness distribution across the thickness. These two properties govern the global in-plane and flexural behavior. Results show that both elasticities decrease strongly with temperature. Higher grading index also softens the structure, since the metal-rich region becomes more dominant at elevated temperature. The study also shows that the TPMS core plays a major role. A higher TPMS filling ratio increases membrane stiffness and raises bending rigidity. At the same time, Poisson's ratio becomes smaller, and thermal conductivity decreases as the core becomes more porous. Thermal expansion is influenced mainly by the grading index. Benchmark comparisons confirm the accuracy of the present model. The predicted thermal buckling temperatures agree well with previous higher-order theories. The study provides trends for how temperature, gradation, and TPMS architecture jointly shape membrane and bending elasticity.

TPMS Çekirdek Katmanlı FDM Sandviç Plakanın Tasarımı ve Termo Elastik Davranışı

Makale Bilgisi

Araştırma makalesi
Başvuru: 13/12/2025
Düzeltme: 23/02/2026
Kabul: 04/03/2026

Anahtar Kelimeler

Sandviç Plaka
TPMS
FDM
Malzeme Özellikleri

Öz

Bu çalışma, fonksiyonel olarak derecelendirilmiş (FDM) yüzey tabakalarına ve TPMS (Triply Periodic Minimal Surface) çekirdeğe sahip bir sandviç plakanın termo-mekanik davranışını incelemektedir. Yüzey tabakaları Si_3N_4/SUS304 malzemelerinden oluşmakta ve güç yasasına dayalı bir dağılım izlemektedir. Primitive, Gyroid ve IWP TPMS yapıları, homojenleştirilmiş Gibson–Ashby ilişkileri kullanılarak modellenmiştir. Tüm tabakalar için sıcaklığa bağlı elastik ve termal malzeme özellikleri dikkate alınmıştır. Analiz, malzeme derecelendirme indeksi, sıcaklık artışı ve TPMS hacim doluluk oranının sandviç plakanın efektif membran elastisite modülü ve efektif eğilme elastisite modülü üzerindeki etkilerine odaklanmaktadır. Homojen tek katmanlı bir plakada, düzlem içi (membran) ve eğilme tepkileri birbirinden bağımsızdır ve kalınlık boyunca bir rijitlik dağılımı tarafından belirlenir. Buna karşılık, sandviç yapılar gibi daha yumuşak bir çekirdeğe sahip plakalarda, kalınlık boyunca rijitliğin düzgün olmaması nedeniyle etkin membran ve eğilme elastisite modülleri birbirinden farklılaşmaktadır. Bu iki elastik özellik, yapının genel düzlem içi ve eğilme davranışını belirlemektedir. Sonuçlar, her iki elastisite modülünün de sıcaklık arttıkça belirgin şekilde azaldığını göstermektedir. Malzeme derecelendirme indeksinin artması da, yüksek sıcaklıklarda metal ağırlıklı bölgenin baskın hâle gelmesi nedeniyle yapının yumuşamasına yol açmaktadır. Çalışma ayrıca TPMS çekirdeğin belirleyici bir rol oynadığını ortaya koymaktadır. TPMS doluluk oranının artması, membran rijitliğini artırmakta ve eğilme rijitliğini yükseltmektedir. Aynı zamanda, çekirdek daha boşluklu hâle geldikçe Poisson oranı azalmakta ve ısıl iletkenlik düşmektedir. Isıl genleşme ise esas olarak malzeme derecelendirme indeksinden etkilenmektedir. Doğrulama çalışmaları, sunulan modelin doğruluğunu teyit etmektedir. Hesaplanan termal burkulma sıcaklıkları, daha önce geliştirilen yüksek mertebeli teorilerle iyi bir uyum göstermektedir. Bu çalışma, sıcaklık, derecelendirme indeksi ve TPMS geometrisinin birlikte membran ve eğilme rijitliklerinden kaynaklanan elastisite modüllerinin nasıl şekillendirdiğine dair genel eğilimleri ortaya koymaktadır.

*Corresponding author, e-mail: ademfatih.ozalp@yalova.edu.tr
DOI: 10.29109/gujsc.1841430

1. INTRODUCTION (GİRİŞ)

Engineering structures benefit from materials whose behavior can be adjusted according to the design. Consequently, advanced materials such as alloys, composites, and functionally graded materials (FGMs) have been developed. In FGMs, the material does not stay the same through the thickness. The properties vary gradually through the thickness, which prevents the abrupt discontinuities observed in layered plates. This smooth variation significantly reduces interfacial stress concentrations. [1].

The gradual shift from ceramic to metal helps cut the thermal stresses that come from their different expansion rates. This feature is particularly important in aerospace and fusion applications. FGMs are now used in many of these areas, including fusion plants, aircraft components, and chemical equipment. Their use keeps increasing, mainly because engineers can adjust stiffness, strength, and thermal behavior by changing the material mix [2]. They are also light and show good resistance to heat. This characteristic becomes especially beneficial at micro- and nano-scales. With these features, FGMs often give reliable performance in very small structures [3].

The amount of ceramic in the mix has a strong effect on how the material reacts to thermal load. With more ceramic, the FGM can handle higher temperatures and stays more stable under heavy heating [4]. Key thermomechanical features like buckling temperature, stress levels, and overall deformation change noticeably with the gradation index and the shape of the plate. Because of this, the structure must be modelled carefully when thermal loads are present [5]. Before running costly experiments, researchers often study these systems with theoretical tools such as classical plate theory, first-order shear deformation theory, and higher-order shear deformation theory.

Classical plate theory (CPT) does not include transverse shear. Because of that, it often predicts stiffness that is too high for thick FG plates. This also makes its thermal buckling estimates unreliable for medium or large thickness plates [5]. First-order shear deformation theory (FSDT) adds shear effects, but it depends on shear-correction factors. These factors introduce uncertainty and can reduce the overall reliability of the model [6].

Higher-order shear deformation theories (HSDT) help address these issues. Reddy-type HSDT gives a realistic parabolic shear-strain shape and does not require shear-correction factors. Because of this, these models provide better predictions for bending, vibration, and thermal behavior in FG plates [7]. Some newer forms of HSDT also include thickness stretching, which makes the model more realistic for FG sandwich beams and plates. These approaches improve accuracy when the structure faces both thermal and mechanical loads [8].

New shear functions have been introduced to improve nonlinear thermal buckling predictions for FG circular plates. They give a more accurate displacement field, especially when the temperature varies across the plate [9]. Quasi-3D theories expand on this idea by adding transverse normal deformation. With this extra term, they often predict vibration and bending behavior more accurately than standard 2D HSDT models [7].

Carrera's Unified Formulation (CUF) provides one framework that can represent many plate and shell theories. It helps model complex FG parts and gives more accurate thermo-mechanical results with fewer assumptions [10]. At very small scales, classical elasticity fails because it does not include size effects. Nonlocal elasticity solves this and gives better predictions for FG nanobeams and nanoshells under thermal loads [3].

To improve FGM response against demanding conditions sandwich plates are made of FGM surface plates and different core geometries. Different core types show different benefits. Solid cores give high strength but do not offer the low weight of other options. Foam cores, on the other hand, cut weight and improve impact resistance because of their cellular layout [11,12]. Studies show that foam cores can strongly change the stiffness and deflection of sandwich panels, and shear effects may make up as much as 93% of the total deflection [11]. Porous cores are another option. Their small voids improve certain dynamic behaviors and work well in systems that need good energy absorption [13,14].

Honeycomb cores are common because they are light and efficient. They have high strength-to-weight ratio and can improve vibration with dynamic loads. Some honeycomb designs also show a near-zero Poisson's ratio. It is helpful in systems that need shape changes [15]. Re-entrant and hexachiral patterns have gained interest as well. Their unique mechanical behavior provides bending and torsional stiffness raise [16,17].

Triply periodic minimal surfaces (TPMS) have become an important core option. Their cell shapes

can be optimized to give high strength and keeping the weight low. Experimental studies indicate that TPMS cores can outperform honeycomb cores due to their more efficient load transfer mechanisms. Because they carry loads more efficiently [18–20]. They also influence bending stiffness and energy absorption in sandwich panels. These complex designs can be produced more easily with additive manufacturing [18,19]. Their geometry can have a high stiffness-to-weight ratio and good energy absorption [21,22].

Design changes can raise their performance further; graded TPMS beams increase bending strength and SEA, DX lattices show much higher energy absorption, and hybrid forms improve crushing behavior and efficiency [23–26]. TPMS plates also keep stiffness well and reach higher natural frequencies, while particular porosity can increase specific stiffness [27,28]. Fast modelling tools and machine-learning methods now allow quick and accurate dynamic predictions with greatly reduced computing time [22,29,30]. IWP-type TPMS structures also give better vibration damping in the 250–450 Hz range [31]. Their open pore layout improves sound absorption, especially in hybrid P+N forms [32,33]. Diamond TPMS shapes enhance heat transfer, although non-TPMS lattices may show better thermal-hydraulic efficiency due to lower flow resistance [34]. FG-TPMS structures also show strong thermo-mechanical stability and can greatly increase critical thermal buckling loads, though CNT agglomeration may reduce frequencies under temperature change [35,36].

The novelty of this study lies in combining TPMS lattice cores with functionally graded face sheets within a unified thermo-elastic framework. Most existing studies mainly focus on displacement, strength, or vibration behavior. In the present work, both membrane and bending elastic responses are evaluated simultaneously, providing a clearer understanding of the global stiffness behavior of sandwich structures. In addition, three TPMS topologies (Primitive, Gyroid, and IWP) are examined under identical modeling conditions, allowing a consistent comparison of geometric effects. The study also highlights membrane–bending coupling caused by stiffness variation through the thickness, which has received limited attention in previous TPMS–FGM sandwich studies.

2. SANDWICH STRUCTURE (SANDVİÇ YAPI)

2.1. Face Layers (Yüzey Katmanları)

The face layers are made from FGMs, where the mechanical and thermal properties change smoothly through the thickness. In this study, the FGM is formed by combining ceramic and metal phases (Figure 1). Their effective properties are determined using the rule of mixtures as commonly done in earlier works [37,38].

The face sheets are arranged in a symmetric manner so that the ceramic phase always appears on the outer surfaces. The effective properties of the upper and lower layers can therefore be taken as identical and are given as follows:

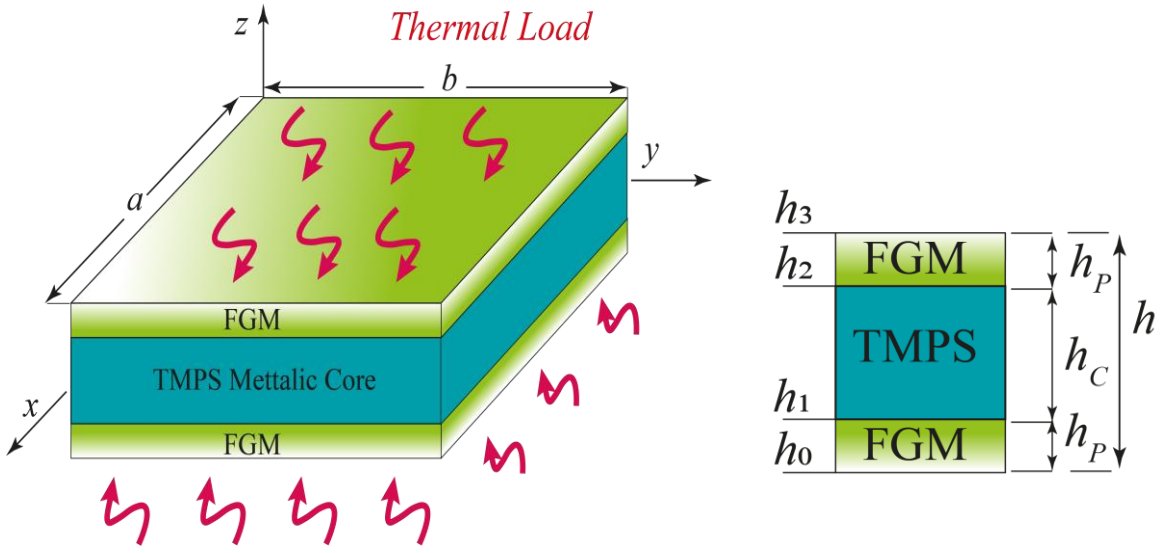

Figure 1. Notation of the geometric dimensions for the sandwich plate and the TPMS core geometry
(Sandviç plaka ve TPMS çekirdek geometrisinin geometrik boyutlarının gösterimi)

$h_f = (h - h_c)/2$

Top Layer:

$$P(z) = P_m + (P_c - P_m)\left(\frac{z - h_c/2}{h_f}\right)^n \quad (1)$$

$(h_c/2 \le z \le h/2)$

Bottom Layer:

$$P(z) = P_m + (P_c - P_m)\left(\frac{-z-h_c/2}{h_f}\right)^n \quad (2)$$

$(-h/2 \le z \le -h_c/2)$

The function $P(z)$ is used to express the variation of material properties, such as the elastic modulus E, shear modulus G, Poisson's ratio v, and density ρ. The symbols m and c refer to the metal and ceramic phases. In this formulation, $z$represents the thickness coordinate, h is the total thickness of the sandwich plate, and n denotes the power-law index.

The material grading index (n) defines how the ceramic and metal volume fractions change across the thickness of the FGM face layers. It controls the gradual transition between ceramic-rich and metal-rich regions. Small values of n produce a ceramic-dominant distribution through a larger thickness. This leads to higher stiffness, lower thermal expansion, and better thermal resistance. Larger values of n increase the metal content. As a result, stiffness decreases while ductility becomes more pronounced. Therefore, the grading index is an important design parameter used to adjust the thermo-mechanical behavior of the sandwich structure according to engineering needs.

2.2. Geometric configuration of the TPMS lattice structure (TPMS Kafes Yapısının Geometrisi)

Core plate is composed of TPMS structure and three different types are used (Figure 3). This section outlines the basic formulation used for various TPMS types. Using the Weierstrass method [39], the following expressions are obtained:

$$\alpha = Re\int_{\Omega_0}^{\Omega_1} e^{i\theta}(1-\Omega^2)R(\Omega)d\Omega \quad (3)$$

$$\beta = Re\int_{\Omega_0}^{\Omega_1} e^{i\theta}(1+\Omega^2)R(\Omega)d\Omega \quad (4)$$

$$z = Re\int_{\Omega_0}^{\Omega_1} e^{i\theta}(2\Omega)R(\Omega)d\Omega \quad (5)$$

In this expression, Ω represents a complex variable, $R(\Omega)$ is the surface function, and θ is the Bonnet angle. The position of any point on the surface is given by the real part of the Re (contour integral). However, this formulation has certain restrictions depending on the TPMS type. Therefore, the following relation is adopted:

$$\psi(r) = \sum_{k=1}^{k} A_k \cos\left[\frac{2\pi(h_k r)}{\lambda_k} + P_k\right] = C \quad (6)$$

Eq. 6 gives a level-set form of several periodic surfaces using a Fourier series. In this relation, r is the position vector, h_k is the k-th reciprocal-space grid vector, and A_k is the corresponding amplitude. The terms P_k and λ_k represent the phase shift and the periodic wavelength. The constant C controls the offset of the implicit surface. By adjusting C together with the substitutions $X = 2\pi\alpha$, $Y = 2\pi\beta$, and $Z = 2\pi z$, different TPMS geometries can be generated.

The relative density (RD) is defined as the ratio of V_{TPMS} (the volume enclosed by the isosurface) to V_{solid} (the total cube volume) [40]. This value determines the wall thickness of the core and strongly influences the overall performance. Therefore, RD is treated as an important design parameter in TPMS lattice structures.

The TPMS cores are modeled as homogenized cellular solids. The effective Young's modulus E_{core}, shear modulus G_{core} and Poisson's ratio ν_{core} are expressed as Gibson–Ashby–type power-law functions of the relative density V, based on previously reported numerical/experimental homogenization data for Primitive, Gyroid and IWP TPMS architectures. In the present study, E_m, G_m and ν_m denote the temperature-dependent elastic properties of the fully dense SUS304 matrix, while here V represents the solid volume fraction of the TPMS core and later it is presented as V_{TPMS} in the analysis [41].

Primitive TPMS (Model I)

$$\left.\begin{matrix} E = E^m(0.317V^{1.264}) \\ G = G^m(0.705V^{1.189}) \end{matrix}\right], \quad V \le 0.25 \quad (7)$$

$$\left.\begin{matrix} E = E^m(1.007V^{2.006} - 0.007) \\ G = G^m(0.953V^{1.715} + 0.047) \end{matrix}\right], \quad V > 0.25 \quad (8)$$

$$\left.\begin{matrix} v = v^m(0.314e^{-1.004V} + 0.119) & V \le 0.55 \\ v = v^m(0.152V^2 - 0.235V + 0.383) & V > 0.55 \end{matrix}\right] \quad (9)$$

Gyroid TPMS (Model II)

$$\left.\begin{matrix} E = E^m(0.596V^{1.467}) \\ G = G^m(0.777V^{1.544}) \end{matrix}\right], V \le 0.45 \quad (10)$$

$$\left.\begin{matrix} E = E^m(0.962V^{2.006} + 0.038) \\ G = G^m(0.973V^{1.982} + 0.027) \end{matrix}\right], V > 0.45 \quad (11)$$

$$\left.\begin{matrix} v = v^m(0.192e^{-1.349V} + 0.202) & V \le 0.50 \\ v = v^m(0.402V^2 - 0.603V + 0.501) & V > 0.50 \end{matrix}\right] \quad (12)$$

IWP TPMS (Model III)

$$\left.\begin{matrix} E = E^m(0.597V^{1.225}) \\ G = G^m(0.529V^{1.287}) \end{matrix}\right], \quad V \le 0.35 \quad (13)$$

$$\left.\begin{matrix} E = E^m(0.987V^{1.782} + 0.013) \\ G = G^m(0.960V^{2.188} + 0.040) \end{matrix}\right], \quad V > 0.35 \quad (14)$$

$$v = \begin{matrix} v^m(2.597e^{-0.157V} - 2.244) \\ v^m(V^2 - V) \end{matrix}\Bigg], \quad \begin{matrix} V \leq 0.13 \\ V > 0.13 \end{matrix} \tag{15}$$

2.3. Temperature Field (Sıcaklık Profili)

The uniform, linear, and nonlinear temperature distributions along the z axis of the FG sandwich plate are evaluated by assuming an initial, stress-free temperature of $T_i = 300$ K. The plate is then heated uniformly to a final temperature T. This process can be expressed as follows:

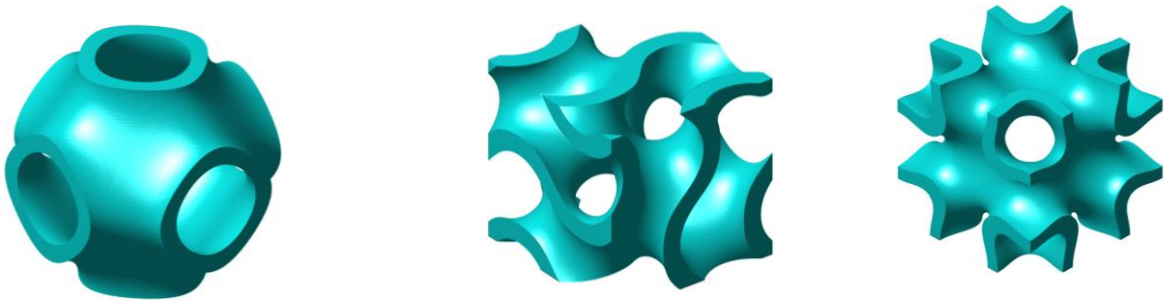

a) b) c)

Figure 2. a) Primitive model, b) Gyroid model, c) IWP model

Table 1. Material properties for Si_3N_4 and SUS304 [42] (Si_3N_4 ve SUS304 için malzeme özellikleri)

Material	Property	$\mathcal{H}_{-1}$	$\mathcal{H}_0$	$\mathcal{H}_1$	$\mathcal{H}_2$	$\mathcal{H}_3$
Si_3N_4	E(Pa)	0	348.43x10^{9}	-3.070x10^{-4}	2.160x10^{-7}	-8.946x10^{-11}
	v	0	0.24	0	0	0
	α(K^{-1})	0	5.8723x10^{-6}	9.095x10^{-4}	0	0
	κ(W/mK)	0	13.723	-1.032x10^{-3}	5.466x10^{-7}	-7.876x10^{-11}
	ρ(kg/m^3)	0	2370	0	0	0
SUS304	E(Pa)	0	201.04x10^{9}	3.079x10^{-4}	-6.534x10^{-7}	0
	v	0	0.3262	-2.002x10^{-4}	3.797x10^{-7}	0
	α(K^{-1})	0	12.330x10^{-6}	8.086x10^{-4}	0	0
	κ(W/mK)	0	15.379	-1.264x10^{-3}	2.092x10^{-6}	-7.223x10^{-10}
	ρ(kg/m^3)	0	8166	0	0	0

Table 2. For $n = 2$, $\xi = 5$, and $\alpha = 0.3$, the buckling temperature of an FGM sandwich plate, SSSS.
(n =2, $\xi = 5$ ve $\alpha = 0.3$, için, bir FGM sandviç plakanın kritik burkulma sıcaklığı, SSSS.)

Type	a/H	ΔT_{cr}					
		Present study	Radwan [46]	Zenkour and Sobhy [43]	Chedad et al. [45]	Reddy [44]	Zenkour and Sobhy [43]
1-0-1	5	23.02568	23.00135	23.0683	23.0137	23.02926	23.0683
	10	6.12530	6.12245	6.12734	6.12335	6.12449	6.12734
	15	2.64905	2.64759	2.64858	2.64777	2.648	2.64858
	25	0.82124	0.82102	0.82115	0.82105	0.82107	0.82115
	50	0.04054	0.04051	0.04051	0.04051	0.04052	0.04051
2-1-2	5	22.37587	22.33166	22.38252	22.34097	22.35275	22.38252
	10	5.89928	5.89686	5.90053	5.89754	5.89838	5.90053
	15	2.53455	2.53458	2.53532	2.53472	2.53488	2.53532
	25	0.77013	0.77007	0.77017	0.77009	0.77011	0.77017
	50	0.01668	0.01668	0.01668	0.01668	0.01668	0.01668
1-1-1	5	21.97308	21.97101	22.00152	21.97619	21.98303	22.00152
	10	5.81195	5.81161	5.81379	5.81198	5.81247	5.81379
	15	2.49780	2.49738	2.49783	2.49746	2.49756	2.49783
	25	0.75654	0.75698	0.75703	0.75699	0.75699	0.75703
	50	0.01363	0.01363	0.01363	0.01363	0.01363	0.01363
1-2-1	5	21.54685	21.54827	21.54917	21.54722	21.54679	21.54917
	10	5.75366	5.75383	5.7538	5.75373	5.75368	5.7538
	15	2.48205	2.48206	2.48205	2.48203	2.48202	2.48205
	25	0.75946	0.75946	0.75946	0.75946	0.75946	0.75946
	50	0.0228	0.02279	0.02279	0.02279	0.02279	0.02279

$$\Delta T = T - T_i \tag{16}$$

Because the temperature gradient changes linearly, the temperature field through the thickness can be written as a linear function.

$$T(z) = T_i + \Delta T\left(\frac{z}{h} + \frac{1}{2}\right) \tag{17}$$

The one-dimensional steady-state heat conduction equation for a nonlinear temperature profile through the plate thickness is written as follows:

$$\frac{d}{dz}\left(\kappa(z,T)\frac{dT}{dz}\right) = 0, \quad T\left(\frac{h}{2}\right) = T_t, \quad T\left(-\frac{h}{2}\right) = T_b \tag{18}$$

Here z=0 on mid-plane

Top Layer , $z \in [h_c/2, h/2]$

$$\kappa(z,T) = \kappa_m(T) + \big(\kappa_c(T) - \kappa_m(T)\big)V_c(z), \quad V_c(z) = \left(\frac{2z-h_c}{h-h_c}\right)^n \tag{19}$$

$$\int_{T_i}^{T_z}\Big[\kappa_m(T) + \big(\kappa_c(T) - \kappa_m(T)\big)V_c(z)\Big]dT \tag{20}$$

Core Layer, $z \in [-h_c/2, h_c/2]$

$$\kappa_{core}(T) = V_m\,\kappa_m(T) \tag{21}$$

$$\int_{T_i}^{T_z}\kappa_{core}(T)dT \tag{22}$$

Bottom Layer $z \in [-h/2, -h_c/2]$

$$\kappa(z,T) = \kappa_m(T) + \big(\kappa_c(T) - \kappa_m(T)\big)V_c(z), \quad V_c(z) = \left(\frac{-2z-h_c}{h-h_c}\right)^n \tag{23}$$

$$\int_{T_i}^{T_z}\Big[\kappa_m(T) + \big(\kappa_c(T) - \kappa_m(T)\big)V_c(z)\Big]dT \tag{24}$$

$$\mathcal{H}(T) = \mathcal{H}_0\,(\mathcal{H}_{-1}T^{-1} + 1 + \mathcal{H}_1 T + \mathcal{H}_2 T^2 + \mathcal{H}_3 T^3) \tag{25}$$

$\mathcal{H}$ represents any temperature-dependent material property, such as Poisson's ratio ν, thermal expansion α, density ρ, thermal conductivity κ, or elastic modulus E. The coefficients listed in Table 1 are used to compute $\mathcal{H}(T)$ for a given temperature.

2.4. **Stress–Strain Relation** (Gerilme–Deformasyon İlişkisi)

This is the stress–strain relation of an isotropic layer under plane-stress conditions. The stiffness matrix $Q(z)$ depends on the local material properties at thickness coordinate z.

$$\begin{bmatrix}\sigma_x\\ \sigma_y\\ \tau_{xy}\end{bmatrix} = Q(z)\begin{bmatrix}\varepsilon_x\\ \varepsilon_x\\ \gamma_{xy}\end{bmatrix} \tag{26}$$

$$Q^{(k)} = \begin{bmatrix}Q_{11} & Q_{12} & 0\\ Q_{21} & Q_{22} & 0\\ 0 & 0 & Q_{66}\end{bmatrix} \tag{27}$$

$$Q_{11} = Q_{22} = E(z)/(1-\nu(z)^2), \quad Q_{12} = \big(\nu(z)E(z)\big)/(1-\nu(z)^2), \quad Q_{66} = 2E(z)/(1-\nu(z)^2) \tag{28}$$

These equations (Eq. 28) define the reduced stiffness matrix of each layer based on its effective $E(z)$, $\nu(z)$, and $G(z)$.

$$A = \sum_{n=1}^{3}\int_{h_{n-1}}^{h_n} Q(z)dz \tag{29}$$

$$B = \sum_{n=1}^{3}\int_{h_{n-1}}^{h_n} z\,Q(z)dz \tag{30}$$

$$D = \sum_{n=1}^{3}\int_{h_{n-1}}^{h_n} z^2 Q(z)dz \tag{31}$$

Matrices A, B and D represent membrane stiffness, membrane–bending coupling and bending stiffness, respectively.

$$\tilde{Q}_{11}^m = A_{11}/h_{tot}, \quad \tilde{Q}_{12}^m = A_{12}/h_{tot}, \quad \tilde{Q}_{66}^m = A_{66}/h_{tot} \tag{32}$$

$$\nu_m = \tilde{Q}_{12}^m/\tilde{Q}_{11}^m, \quad E_m = (1-\nu_m^2)\tilde{Q}_{11}^m, \quad G_m = \tilde{Q}_{66}^m \tag{33}$$

Eq. 34 gives effective in-plane elastic properties of the sandwich. Also E_b is effective bending elasticity property and α_{mem} is effective membrane thermal expansion coefficient.

$$\tilde{Q}_{11}^b = 12D_{11}/h_{tot}^3, \quad \tilde{Q}_{12}^b = 12D_{12}/h_{tot}^3, \quad \tilde{Q}_{66}^b = 12D_{66}/h_{tot}^3, \quad E_b = (1-\nu_m^2)\tilde{Q}_{11}^b \tag{34}$$

$$\alpha^{(k)} = \begin{bmatrix}\alpha_k\\ \alpha_k\\ 0\end{bmatrix}$$

$$A_\alpha = \sum_{n=1}^{3}\int_{h_{n-1}}^{h_n}\alpha\,Q(z)dz \tag{35}$$

$$A_{11}\alpha_{mem}\Delta T = A_{\alpha,11}\,\Delta T$$

$$\alpha_{mem} = A_{\alpha,11}/A_{11}$$

2.5. Verification (Doğrulama)

The present study was validated by comparing its outcomes with previously published results (Table 2). These comparison tables indicate that the numerical predictions obtained here are consistent with earlier works employing higher-order plate formulations under SSSS boundary conditions. Results generated using CPT, FSDT, and the advanced theories developed by Zenkour and Sobhy [43], Reddy [44], Chedad et al. [45], and Radwan [46] were placed alongside the current findings. Among these, the present results show particularly close agreement

3. RESULTS (BULGULAR)

A rectangular sandwich plate measuring 1m x 1m in plane dimensions with thickness $h = a/10$ is taken as the structural model. The outer layers are composed of functionally graded Si_3N_4/SUS304, and the core is formed by a SUS304 TPMS geometry. Analysis show the effect of material grading index and volume of TPMS on the material properties such as elasticity modulus derived from in-plane (membrane) and bending, shear elasticity, Poisson's ratio, thermal expansion ratio and thermal conductivity.

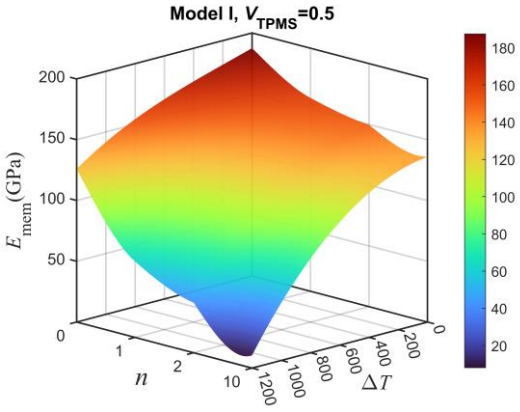

a)

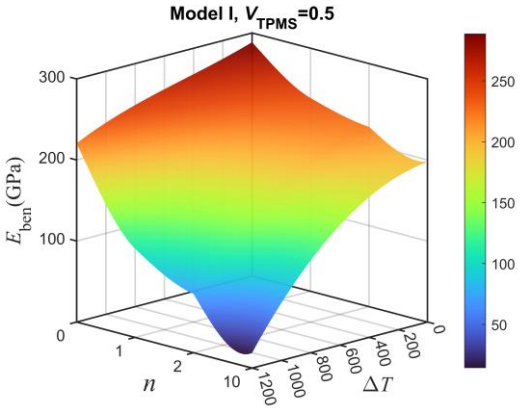

b)

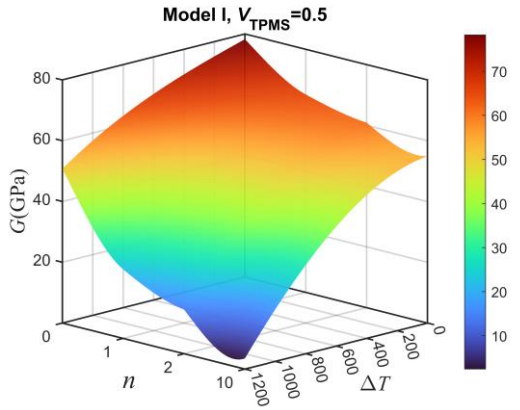

c)

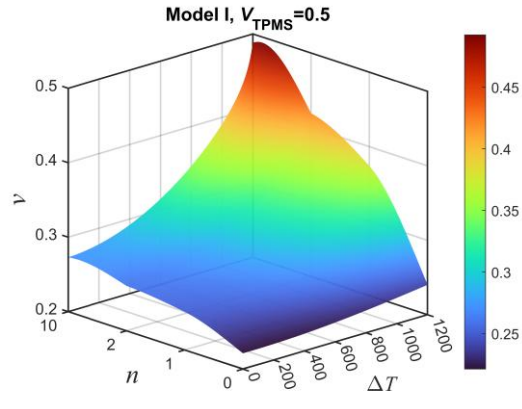

d)

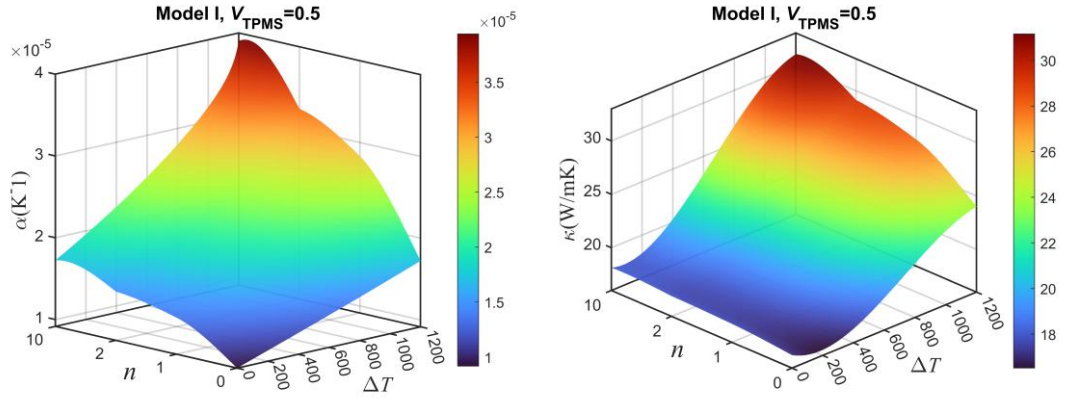

e) f)

Figure 1. The influence of the material grading index on a) membrane stiffness, b) bending stiffness, c) shear stiffness, d) Poisson's ratio, e) thermal expansion, and f) thermal conductivity (Malzeme derecelendirme indeksinin a) membran elastisitesi, b) eğilme elastisitesi, c) kayma gerilmesi, d) Poisson oranı, e) termal genleşme ve f) termal iletkenlik üzerindeki etkisi)

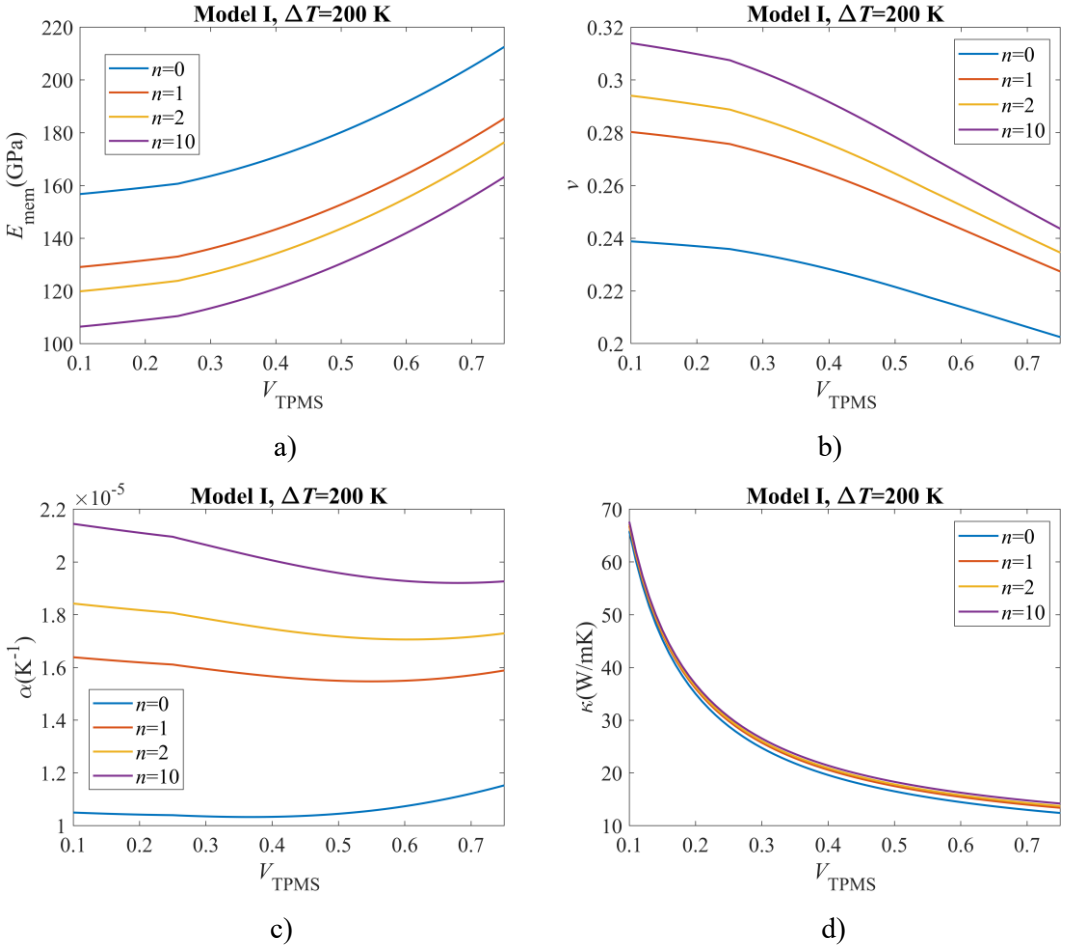

a) b)

c) d)

Figure 2. The influence of the material grading index, together with the TPMS volume filling ratio, on the material properties of the sandwich plate and Core Model I is examined for: a) membrane stiffness, b) Poisson's ratio, c) thermal expansion, and d) thermal conductivity (Malzeme derecelendirme indeksinin, TPMS hacim doluluk oranıyla birlikte, sandviç plaka ve Çekirdek Model I'in malzeme özelliklerine etkisi: a) membran elastisitesi, b) Poisson oranı, c) termal genleşme ve d) termal iletkenlik)

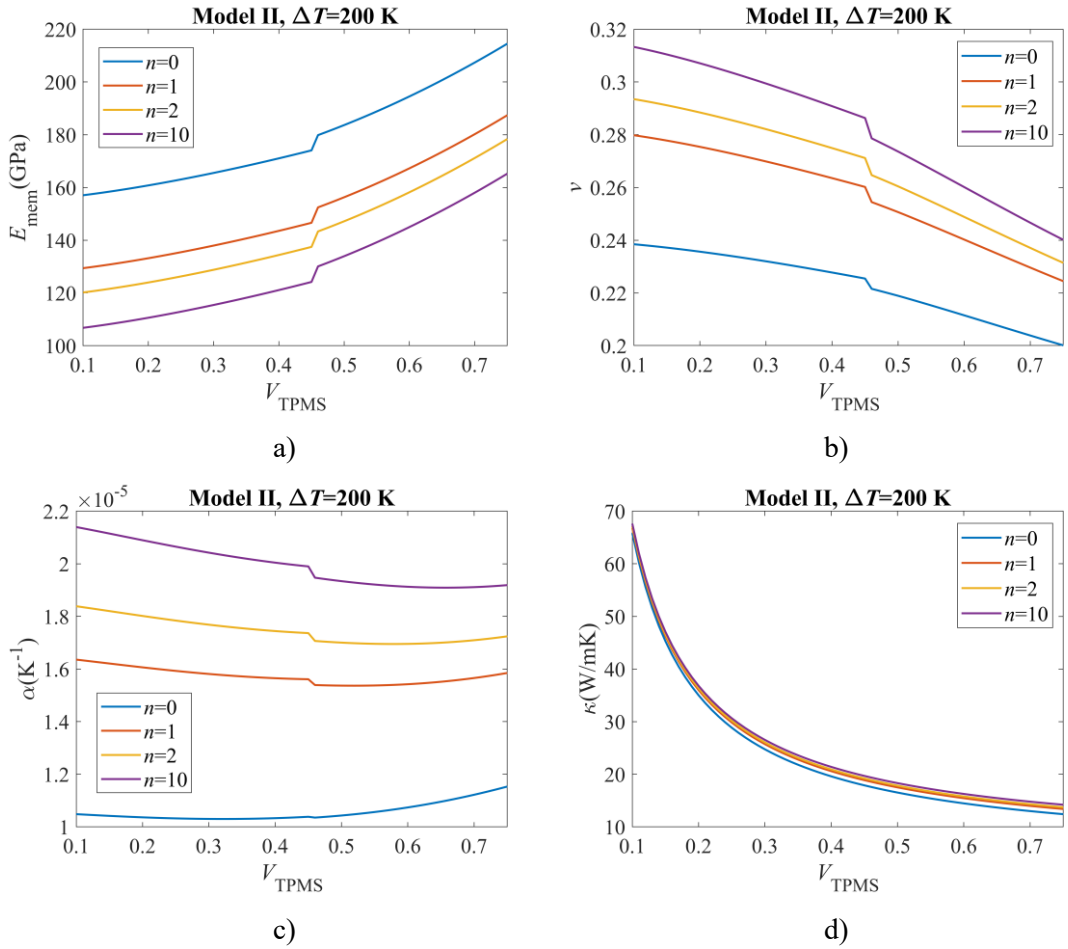

Figure 3. The influence of the material grading index, together with the TPMS volume filling ratio, on the material properties of the sandwich plate and Core Model II is examined for: a) membrane stiffness, b) Poisson's ratio, c) thermal expansion, and d) thermal conductivity (Malzeme derecelendirme indeksinin, TPMS hacim doluluk oranıyla birlikte, sandviç plaka ve Çekirdek Model II'nin malzeme özelliklerine etkisi: a) membran elastisitesi, b) Poisson oranı, c) termal genleşme ve d) termal iletkenlik)

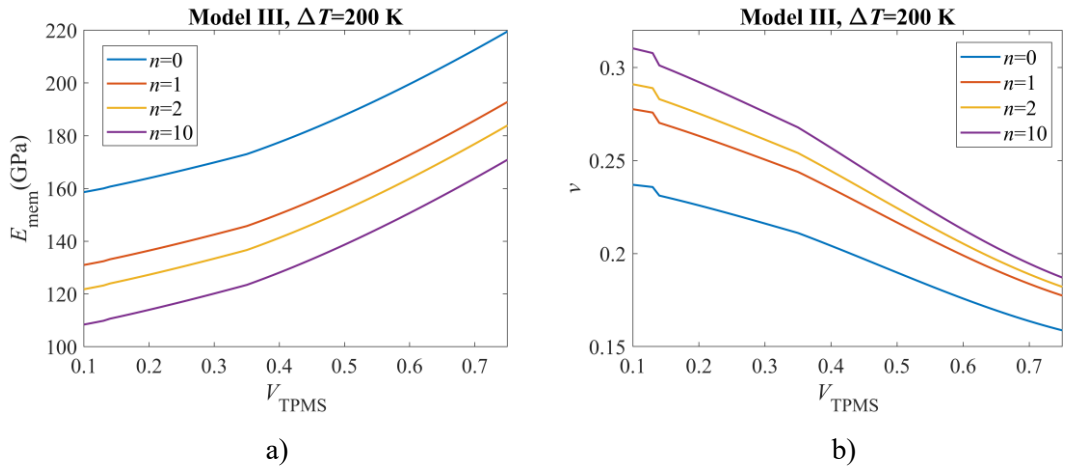

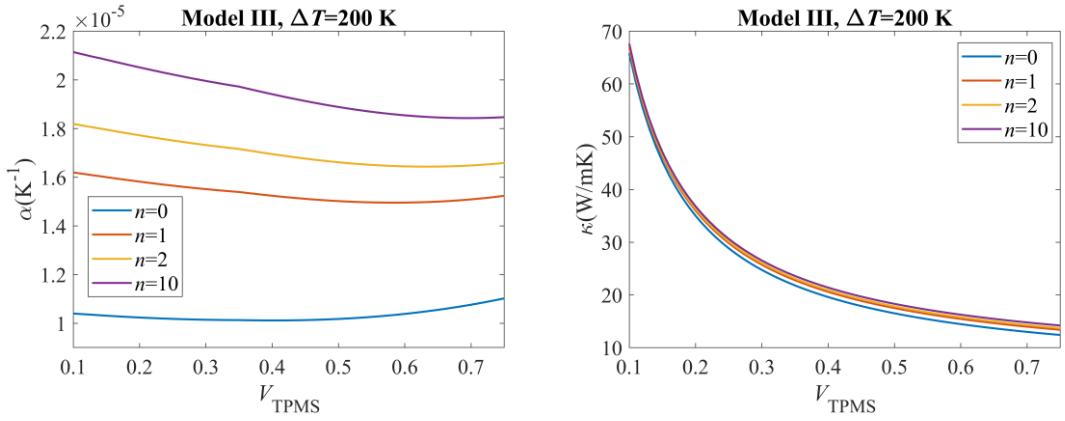

Figure 4. The influence of the material grading index, together with the TPMS volume filling ratio, on the material properties of the sandwich plate and Core Model III is examined for: a) membrane stiffness, b) Poisson's ratio, c) thermal expansion, and d) thermal conductivity (Malzeme derecelendirme indeksinin, TPMS hacim doluluk oranıyla birlikte, sandviç plaka ve Çekirdek Model III'ün malzeme özelliklerine etkisi: a) membran elastisitesi, b) Poisson oranı, c) termal genleşme ve d) termal iletkenlik)

In a homogeneous single-layer plate, the stress field is dominated by classical bending behavior, and significant membrane stresses do not arise under symmetric transverse loading. However, when the structure is configured as a sandwich plate with FGM face sheets and a TPMS core, the through-thickness stiffness becomes highly non-uniform. The face layers carry most of the in-plane stiffness, while the TPMS core provides shear rigidity and increases the distance between the face sheets. This mechanical discontinuity leads to bending–membrane coupling, a characteristic response of multilayer sandwich systems. As a result, both bending stresses (σ_x^b, σ_γ^b) and membrane stresses (σ_x^0, σ_γ^0) develop in the FGM face layers even under loading conditions where a single layer plate would exhibit negligible in-plane stress. The TPMS core amplifies this effect by modifying the neutral axis position and redistributing the stress field across the thickness.

3.1. Effect of the Material Grading Index on Material Properties (Malzeme Gradyan İndeksinin Malzeme Özellikleri Üzerindeki Etkisi)

Figure 3(a) shows the variation of the equivalent in-plane Young's modulus E_{mem} with respect to the material grading index $n$and the temperature rise ΔT. For $n = 0$, E_{mem} starts at approximately 187.5 GPa at $\Delta T = 0$ and decreases almost linearly to about 125.8 GPa at $\Delta T = 1200$K, corresponding to a 33% reduction. For moderate grading ($n \approx 1$), the modulus decreases from nearly 178–180 GPa down to 115–120 GPa, indicating a comparable softening trend. The lowest stiffness occurs at large grading parameters ($n > 2$), where E_{mem} falls below 100 GPa for $\Delta T > 1000$K, reflecting the stronger influence of the metal-rich region under thermal degradation.

Figure 3(b) depicts the variation of the equivalent bending Young's modulus $E_{\text{ben}}$with the material grading index $n$and the temperature rise ΔT. For $n = 0$, E_{ben} is about 288.6 GPa at $\Delta T = 0$ and decreases to nearly 224.1 GPa at $\Delta T = 1200$K, corresponding to a reduction of roughly 22%. For a moderate grading level ($n \approx 1$), the initial bending modulus is around 238.6 GPa and drops to approximately 109.5 GPa, indicating a stronger thermal softening. When the grading index is further increased ($n \approx 2$ and above), E_{ben} decreases from about 221.9 GPa down to 72.5 GPa, and for the highest considered $n$it falls from 197.7 GPa to nearly 18.7 GPa at $\Delta T = 1200$K.

Figure 3(c) illustrates the variation of the equivalent in-plane shear modulus $G$with the material grading index $n$and the temperature rise ΔT. For $n = 0$, G is about 78 GPa at $\Delta T = 0$ and decreases to nearly 3.5 GPa at $\Delta T = 1200$K, indicating a stiffness loss of roughly 95 %. For moderate gradation ($n \approx 1$), the shear modulus drops from approximately 65 GPa to 14–15 GPa, while for higher grading indices ($n \gtrsim 2$) the initial values are already lower (about 61–55 GPa at $\Delta T = 0$) and converge to around 17–19 GPa at $\Delta T = 1200$K.

Figure 3(d) presents the variation of the equivalent Poisson's ratio ν with the material grading index $n$and the temperature rise ΔT. For $n = 0$, ν is almost temperature–insensitive, increasing only slightly from about 0.22 at $\Delta T = 0$ to 0.24 at $\Delta T = 1200$K. For a moderate grading ($n \approx 1$), ν increases more

markedly, from 0.25 to roughly 0.37 over the same temperature range. At higher grading indices ($n \approx$ 2–3), the temperature sensitivity becomes pronounced: ν rises from about 0.26–0.27 at $\Delta T = 0$ up to nearly 0.48–0.49 at $\Delta T = 1200$K.

Figure 3(e) illustrates the variation of the equivalent in-plane coefficient of thermal expansion α_{mem} with the material grading index n and the temperature rise ΔT.

For $n = 0$, α_{mem} increases from about $9.2\text{x}10^{-6}\ \text{K}^{-1}$ at $\Delta T = 0$ to roughly $1.72\text{x}10^{-5}\ \text{K}^{-1}$ at $\Delta T = 1200$K. For a moderate gradation ($n \approx 1$), the expansion coefficient rises from $1.36\text{x}10^{-5}\ \text{K}^{-1}$ to about $2.83\text{x}10^{-5}\ \text{K}^{-1}$. For higher grading indices ($n \approx$ 2–3), the response becomes strongly temperature-dependent, with α_{mem} growing from approximately $(1.5–1.7)\text{x}10^{-5}\ \text{K}^{-1}$ up to nearly $(3.2–3.9)\text{x}10^{-5}\ \text{K}^{-1}$.

Figure 3(f) illustrates the variation of the equivalent in-plane thermal conductivity $\kappa$with the material grading index n and the temperature rise ΔT. For $n = 0$, κ slightly decreases from about 17.2 W/mK at $\Delta T = 0$ to a minimum of roughly 16.5 W/mK around $\Delta T \approx 200$K, and then increases consistently up to nearly 24.0 W/mK at $\Delta T = 1200$K. For a moderate gradation ($n \approx 1$), κ rises from 17.7 W/mK to approximately 27.9 W/mK, whereas at higher grading indices ($n \approx$ 2–3) it increases from about 17.9–18.1 W/mK to 29.1–31.0 W/mK.

3.2. Effect of the Material Grading Index and TPMS Volume on Material Properties

(Malzeme Gradyan İndeksi ve TPMS Hacminin Malzeme Özellikleri Üzerindeki Etkisi)

The parametric trends obtained for the primitive TPMS core at $\Delta T = 200$ K reveal a clear thermomechanical trade-off governed jointly by the filling ratio V_{TPMS} and the material grading index n (Figure 4). As V_{TPMS} increases from 0.1 to 0.75, elasticity modulus derived from in-plane (membrane) E_{mem} consistently rises for all grading indices. For instance, the stiffness for $n = 0$ increases from approximately 155–160 GPa to more than 210 GPa, whereas for $n = 10$ it increases from nearly 105 GPa to about 150 GPa. At fixed V_{TPMS}, the modulus decreases consistently with increasing n, indicating that stronger gradation softens the equivalent membrane response; the stiffest configuration corresponds to $n = 0$ with high filling ratios, while the most compliant configuration occurs for $n = 10$ with low filling ratios.

The effective Poisson's ratio ν decreases with increasing V_{TPMS} but increases with the grading index. For $V_{\text{TPMS}} = 0.1$, ν varies from about 0.24 ($n = 0$) to roughly 0.31 ($n = 10$), whereas at $V_{\text{TPMS}} = 0.75$ it drops to a narrower range around 0.21–0.24. A higher TPMS amount makes the deformation act more in the axial direction, so the lateral contraction becomes smaller. When n is larger, the structure shows more transverse deformation. The thermal expansion coefficient α changes only slightly with V_{TPMS}. Each curve has a small dip in the middle range, with a bit higher values at low and high filling levels. The main factor is the grading index. α rises from about $1.1\text{x}10^{-5}\ \text{K}^{-1}$ at $n = 0$ to about $2.1x10^{-5}\ \text{K}^{-1}$ at $n = 10$. This shows that a larger n increases the effect of the material with higher thermal expansion.

In contrast, the thermal conductivity $\kappa$is strongly governed by V_{TPMS} and only marginally affected by n. All curves decay from roughly 65–70 W/mK at low filling ratios to about 12–14 W/mK at $V_{\text{TPMS}} = 0.75$, while the relative spacing between the n-dependent curves remain small.

For the gyroid-type TPMS core in Model II at ΔT=200 K, the effective membrane modulus E_{mem} increases consistently with the TPMS volume fraction V_{TPMS} over the range 0.10–0.75 for all grading indices n (Figure 5). Higher porosity (small V_{TPMS}) gives the lowest stiffness, while increasing the solid gyroid content progressively stiffens the sandwich, and the curves are clearly ordered such that $n = 0$ is the stiffest and $n = 10$ the most compliant. A small kink appears around $V_{\text{TPMS}} \approx 0.45$ on each curve, indicating a change in the relative contribution of the metallic/ceramic phases to the membrane response in this topology. The effective Poisson's ratio ν shows the opposite trend and it decreases with increasing V_{TPMS} and approaches lower values when the gyroid network is denser, while larger $n$leads to systematically higher ν at any fixed volume fraction. The same transition point around $V_{\text{TPMS}} \approx 0.45$ is reflected as a small downward jump in ν, consistent with the corresponding stiffening in E_{mem}. The effective coefficient of thermal expansion αvaries more mildly with V_{TPMS}; for all n it exhibits a gently curved profile with a slight drop near the same critical volume fraction, and larger grading index again produces a higher thermal expansion level. In contrast, the effective thermal conductivity κ is dominated by the volume fraction and is only weakly affected by n. Furthermore, κ decreases strongly and nonlinearly as V_{TPMS} increases, reflecting the reduced heat-conduction pathways as

the gyroid structure becomes more tortuous, while the four curves for $n = 0,1,2,10$ almost coincide over the entire range. The gyroid TPMS core in Model II shows a clear stiffness conductivity trade-off controlled primarily by V_{TPMS}, with the material grading index mainly shifting the elastic and thermomechanical levels but hardly altering the thermal conduction behavior.

For the Model III core, E_{mem} rises steadily as the TPMS volume fraction V_{TPMS} increases. This means the core becomes stiffer when the porosity gets lower. For any fixed V_{TPMS}, larger grading indices ($n = 1,2,10$) give smaller stiffness than $n = 0$. This result shows that increasing material gradation reduces the effective membrane stiffness (Figure 6).

The Poisson ratio shows the reverse behavior. ν becomes smaller when V_{TPMS} increases, but it becomes larger when the grading index increases. This means that a denser IWP core pushes the deformation toward the axial direction, while stronger grading allows more lateral deformation.

The effective thermal expansion α shows a slight curve as V_{TPMS} changes, with a small minimum in the middle range. For all filling levels, α increases steadily from $n = 0$ to $n = 10$. This indicates that material gradation has a stronger influence on thermal expansion than on stiffness.

Thermal conductivity κ drops quickly and steadily as V_{TPMS} increases, and this happens for all grading indices. The curves for different n are almost the same. This shows that heat transfer is controlled mainly by the TPMS volume, while gradation has only a small effect.

The IWP shape separates the roles of the two parameters. V_{TPMS} controls stiffness and conductivity, while n mainly changes the Poisson-related deformation and the thermal expansion. Its effect on conduction and elasticity is small.

4. CONCLUSIONS (SONUÇLAR)

From a practical perspective, the proposed TPMS core can be manufactured using modern additive manufacturing methods. These techniques allow complex lattice geometries with controlled porosity and good geometric precision. FGM face sheets can also be produced using established processes such as powder metallurgy, thermal spraying, and graded deposition. The initial manufacturing cost may be higher than that of conventional cores. However, the high stiffness-to-weight ratio and improved material efficiency can reduce the overall structural cost. For this reason, the proposed sandwich configuration is considered feasible for advanced lightweight engineering applications.

The study shows that temperature, gradation, and TPMS volume fraction strongly modify the mechanical and thermal response of the sandwich plate. The most sensitive quantities are elasticity modulus derived from in-plane (membrane) and bending, which control the in-plane and flexural behavior. Both elasticities decrease as temperature rises (the equivalent membrane modulus decreases by nearly 33%, while the bending modulus shows reductions of about 22% depending on the grading index). At higher grading indices, the response is dominated by the metal phase due to softening effect.

The TPMS core plays a significant structural role. Increasing its filling ratio enhances both membrane stiffness and bending rigidity (for example, membrane stiffness increases from approximately 155–160 GPa to over 210 GPa as the filling ratio rises). The neutral axis shifts, and load transfer between the face sheets improves. As a result, the plate resists deformation more effectively. A lower Poisson's ratio at higher TPMS volume reflects a more axial deformation mode.

Thermal expansion depends mainly on the grading index, while thermal conductivity is controlled by the TPMS volume (thermal conductivity decreases from about 65–70 W/mK to nearly 12–14 W/mK with increasing porosity). Increased porosity in the core leads to a rapid reduction in heat transfer.

Although the general behavior is similar, each TPMS geometry modifies stiffness differently. The IWP core strongly influences Poisson-related deformation, whereas the Primitive and Gyroid cores lead to more distinct changes in membrane stiffness.

The study further explains the mechanism responsible for the development of membrane and bending stresses in the FGM face layers even under symmetric loading. The combination of graded faces and TPMS core produces non-uniform stiffness through the thickness, which leads to membrane–bending coupling. This behavior does not appear in a single homogeneous plate.

Finally, verification with published benchmark results confirms that the present formulation is

accurate. The predicted thermal behavior matches well with advanced shear deformation theories.

DECLARATION OF ETHICAL STANDARDS
(ETİK STANDARTLARIN BEYANI)

The author of this article declares that the materials and methods they use in their work do not require ethical committee approval and/or legal-specific permission.

Bu makalenin yazarı çalışmalarında kullandıkları materyal ve yöntemlerin etik kurul izni ve/veya yasal-özel bir izin gerektirmediğini beyan ederler.

AUTHORS' CONTRIBUTIONS (YAZARLARIN KATKILARI)

***Adem Fatih ÖZALP*:** He constructed the mathematical model and the necessary codes for the analysis, performed the simulations, analyzed the results and wrote the manuscript.

Matematiksel modeli ve analiz için gerekli kodları oluşturmuş, simülasyonları yapmış, sonuçlarını analiz etmiş ve makalenin yazım işlemini gerçekleştirmiştir.

CONFLICT OF INTEREST (ÇIKAR ÇATIŞMASI)

There is no conflict of interest in this study.

Bu çalışmada herhangi bir çıkar çatışması yoktur.

REFERENCES (KAYNAKLAR)

[1] A.J.M. Ferreira, R.C. Batra, C.M.C. Roque, L.F. Qian, P.A.L.S. Martins, Static analysis of functionally graded plates using third-order shear deformation theory and a meshless method, Composite Structures 69 (2005) 449–457. https://doi.org/10.1016/j.compstruct.2004.08.003.

[2] T. Baytak, M. Tosun, C. Ipek, C. Mollamahmutoglu, O. Bulut, Thermal Stress Analysis for Functionally Graded Plates with Modulus Gradation, Part II, Exp Mech 64 (2024) 1229–1247. https://doi.org/10.1007/s11340-024-01091-9.

[3] R. Lal, C. Dangi, Thermomechanical vibration of bi-directional functionally graded non-uniform timoshenko nanobeam using nonlocal elasticity theory, Composites Part B: Engineering 172 (2019) 724–742. https://doi.org/10.1016/j.compositesb.2019.05.076.

[4] S. Trabelsi, A. Frikha, S. Zghal, F. Dammak, Thermal post-buckling analysis of functionally graded material structures using a modified FSDT, International Journal of Mechanical Sciences 144 (2018) 74–89. https://doi.org/10.1016/j.ijmecsci.2018.05.033.

[5] H.V. Tung, N.D. Duc, Thermoelastic stability of thick imperfect functionally graded plates, Vietnam J. Mech. 32 (2010) 47–58. https://doi.org/10.15625/0866-7136/32/1/316.

[6] M. Sid Ahmed Houari, A. Tounsi, O. Anwar Bég, Thermoelastic bending analysis of functionally graded sandwich plates using a new higher order shear and normal deformation theory, International Journal of Mechanical Sciences 76 (2013) 102–111. https://doi.org/10.1016/j.ijmecsci.2013.09.004.

[7] M. Li, C. Guedes Soares, R. Yan, Free vibration analysis of FGM plates on Winkler/Pasternak/Kerr foundation by using a simple quasi-3D HSDT, Composite Structures 264 (2021) 113643. https://doi.org/10.1016/j.compstruct.2021.113643.

[8] R. Bennai, H.A. Atmane, A. Tounsi, A new higher-order shear and normal deformation theory for functionally graded sandwich beams, Steel and Composite Structures 19 (2015) 521–546. https://doi.org/10.12989/SCS.2015.19.3.521.

[9] V.N. Van Do, C.-H. Lee, Nonlinear thermal buckling analyses of functionally graded circular plates using higher-order shear deformation theory with a new transverse shear function and an enhanced mesh-free method, Acta Mech 229 (2018) 3787–3811. https://doi.org/10.1007/s00707-018-2190-7.

[10] D. Li, Z. Deng, H. Xiao, Thermomechanical bending analysis of functionally graded sandwich plates using four-variable refined plate theory, Composites Part B: Engineering 106 (2016) 107–119. https://doi.org/10.1016/j.compositesb.2016.08.041.

[11] L. CoDyre, K. Mak, A. Fam, Flexural and axial behaviour of sandwich panels with bio-based flax fibre-reinforced polymer skins and various foam core densities, Jnl of Sandwich Structures & Materials 20 (2016) 595–616. https://doi.org/10.1177/1099636216667658.

[12] K.G. Aktaş, Analysis of Mechanical and Thermal Material Characteristics of GPL-Reinforced Double-FG Composite Nanoplates under Temperature Load, Gazi Üniversitesi Fen Bilimleri Dergisi Part C: Tasarım ve Teknoloji 13 (2025) 341–354. https://doi.org/10.29109/gujsc.1577831.

[13] E.K. Njim, S.H. Bakhy, M. Al-Waily, Optimisation Design of Functionally Graded Sandwich Plate with Porous Metal Core for

Buckling Characterisations, JST 29 (2021). https://doi.org/10.47836/pjst.29.4.47.

[14] M. Esmaeilzadeh, M.E. Golmakani, Y. Luo, M. Bodaghi, Transient behavior of imperfect bi-directional functionally graded sandwich plates under moving loads, Engineering with Computers 39 (2021) 1305–1315. https://doi.org/10.1007/s00366-021-01521-5.

[15] J. Zhang, Z. Yan, L. Xia, Vibration and Flutter of a Honeycomb Sandwich Plate with Zero Poisson's Ratio, Mathematics 9 (2021) 2528. https://doi.org/10.3390/math9192528.

[16] S. Fan, D. Wang, Bending behavior of uniform and graded TPMS wood-plastic composite sandwich beams, Composites and Advanced Materials 34 (2025). https://doi.org/10.1177/26349833251340994.

[17] V.K. Prajapati, J. Pitchaimani, Flutter behavior of quadrilateral auxetic core sandwich plate with bio-inspired three-phase composite facings numerical analysis and experimental verification, Proceedings of the Institution of Mechanical Engineers, Part L: Journal of Materials: Design and Applications 239 (2024) 490–511. https://doi.org/10.1177/14644207241265465.

[18] N. Iranmanesh, H.Y. Sarvestani, B. Ashrafi, M. Hojjati, Impact performance of 3D printed sandwich structures with specially designed core geometry, Progress in Canadian Mechanical Engineering. Volume 6 (2023). https://doi.org/10.17118/11143/21157.

[19] O. Fashanu, M. Rangapuram, A. Abutunis, J. Newkirk, K. Chandrashekhara, H. Misak, D. Klenosky, Mechanical performance of sandwich composites with additively manufactured triply periodic minimal surface cellular structured core, Jnl of Sandwich Structures & Materials 24 (2021) 1133–1151. https://doi.org/10.1177/10996362211037012.

[20] A. Guo, S. Li, S. Wang, Z. Zhai, P. Qu, S. Guo, H. Kong, R. Tang, L. Wang, W. Meng, C. Liu, Novel triply periodic minimal surfaces sandwich structures: Mechanical performance and failure analysis, Polymer Composites 45 (2024) 11908–11924. https://doi.org/10.1002/pc.28608.

[21] H. Nguyen-Xuan, K.Q. Tran, C.H. Thai, J. Lee, Modelling of functionally graded triply periodic minimal surface (FG-TPMS) plates, Composite Structures 315 (2023) 116981. https://doi.org/10.1016/j.compstruct.2023.116981.

[22] Q. Wang, Q. Yang, R. Zhong, T. Liu, A fast dynamic modeling approach for TPMS lattice sandwich plate, Thin-Walled Structures 218 (2026) 114098. https://doi.org/10.1016/j.tws.2025.114098.

[23] H. Zhang, J. Zhao, C. Xu, R. Huo, Q. Niu, Improving energy absorption in structures using tubular TPMS structure optimization and printing strategies, Composite Structures 377 (2026) 119820. https://doi.org/10.1016/j.compstruct.2025.119820.

[24] H. Wu, D. Li, B. Yang, S. Yu, Improved bending strength and energy absorption in SLM Cu-Cr-Zr lattice-beams using shaped graded TPMS lattice structures, Materials Today Communications 49 (2025) 113687. https://doi.org/10.1016/j.mtcomm.2025.113687.

[25] X. Xiao, L. Yu, X. Zhu, J. Liu, G. Sun, Y. Xu, S. Yang, C. Jiang, D. Geng, J. Zhao, Mechanical performance and energy absorption of Ti6Al4V functionally graded diamond TPMS lattice bionic metamaterials manufactured via selective laser melting, Journal of Materials Research and Technology 39 (2025) 5765–5776. https://doi.org/10.1016/j.jmrt.2025.10.245.

[26] Y. Yin, F. Li, D. Zhu, Enhanced energy absorption characteristics of TPMS lattice structures with linear and circular hybrid designs, Engineering Structures 340 (2025) 120759. https://doi.org/10.1016/j.engstruct.2025.120759.

[27] S. Nosrati, O. Rahmani, S.A. Hosseini, Rapid analysis of bending in curvature-adaptive tpms shells using higher-order shear deformation theory, Mechanics Research Communications 150 (2025) 104577. https://doi.org/10.1016/j.mechrescom.2025.104577.

[28] S. Wang, M. Song, J. Yang, W. Zhu, S. Kitipornchai, Free vibration of functionally graded TPMS porous quadrilateral plates reinforced with graphene nanoplatelets, Thin-Walled Structures 215 (2025) 113440. https://doi.org/10.1016/j.tws.2025.113440.

[29] V.-T. Tran, T.-K. Nguyen, T.P. Vo, A novel hybrid machine learning and optimization approach for stochastic free vibration analysis of graphene platelets reinforced functionally graded triply periodic minimal surface microplates, Engineering Analysis with Boundary Elements 178 (2025) 106304. https://doi.org/10.1016/j.enganabound.2025.106304.

[30] S. Han, Z. Wang, M. El-Meligy, K.A. Alnowibet, Nonlinear dynamic analysis of the

FG-TPMS double-curved panels: Introducing SVM-DNN-RF algorithm to predict nonlinear dynamic information, Aerospace Science and Technology 158 (2025) 109785. https://doi.org/10.1016/j.ast.2024.109785.

[31] C. Zhang, H. Qiao, L. Yang, W. Ouyang, T. He, B. Liu, X. Chen, N. Wang, C. Yan, Vibration characteristics of additive manufactured IWP-type TPMS lattice structures, Composite Structures 327 (2024) 117642. https://doi.org/10.1016/j.compstruct.2023.117642.

[32] K.K. Sirivuri, V. Sekar, W.J. Cantwell, K. Liao, B. Berton, N. Ravaud, P.-M. Jacquart, R.K. Abu Al-Rub, Computational study of sound absorption in TPMS lattice materials using a thermoviscous model, Journal of Building Engineering 112 (2025) 113658. https://doi.org/10.1016/j.jobe.2025.113658.

[33] J.W. Chua, X. Li, W. Zhai, Design, multiscale modelling, and experimental characterisation of TPMS-based composite lattices with enhanced sound absorption, Composite Structures 370 (2025) 119437. https://doi.org/10.1016/j.compstruct.2025.119437.

[34] M. Al-Safadi, S.Z. Shuja, A. Almerbati, S.M. Zubair, CFD benchmarking of triply periodic minimal surface (TPMS) and non-TPMS heat sink geometries: Thermal-hydraulic trade-offs at equal structural volume, International Communications in Heat and Mass Transfer 171 (2026) 110067. https://doi.org/10.1016/j.icheatmasstransfer.2025.110067.

[35] K.Q. Tran, T.V. Duong, T.-D. Hoang, M.A. Wahab, K. Hackl, H. Nguyen-Xuan, A new thermoelastic model for agglomerated and randomly-oriented CNT-reinforced bio-inspired materials: Temperature-dependent free vibration analysis of FG-CNTR-TPMS plates, Engineering Analysis with Boundary Elements 174 (2025) 106157. https://doi.org/10.1016/j.enganabound.2025.106157.

[36] D.T. Dong, T.Q. Minh, B.T. Tu, K.Q. Tran, H. Nguyen-Xuan, Nonlinear thermo-mechanical static stability analysis of FG-TPMS shallow spherical shells, Thin-Walled Structures 205 (2024) 112343. https://doi.org/10.1016/j.tws.2024.112343.

[37] F. Tornabene, Free vibration analysis of functionally graded conical, cylindrical shell and annular plate structures with a four-parameter power-law distribution, Computer Methods in Applied Mechanics and Engineering 198 (2009) 2911–2935. https://doi.org/10.1016/j.cma.2009.04.011.

[38] X. Zhao, Y.Y. Lee, K.M. Liew, Thermoelastic and vibration analysis of functionally graded cylindrical shells, International Journal of Mechanical Sciences 51 (2009) 694–707. https://doi.org/10.1016/j.ijmecsci.2009.08.001.

[39] S. Rajagopalan, R. Robb, Schwarz meets Schwann: Design and fabrication of biomorphic and durataxic tissue engineering scaffolds, Medical Image Analysis 10 (2006) 693–712. https://doi.org/10.1016/j.media.2006.06.001.

[40] S. AlMahri, R. Santiago, D.-W. Lee, H. Ramos, H. Alabdouli, M. Alteneiji, Z. Guan, W. Cantwell, M. Alves, Evaluation of the dynamic response of triply periodic minimal surfaces subjected to high strain-rate compression, Additive Manufacturing 46 (2021) 102220. https://doi.org/10.1016/j.addma.2021.102220.

[41] E. Abdoli, M.R. Zarastvand, R. Talebitooti, Wave propagation numerical simulation approach based on a novel TPMS-based lattice metamaterial for improved vibration transmission of doubly curved sandwich systems, Engineering with Computers 41 (2025) 3737–3754. https://doi.org/10.1007/s00366-025-02181-5.

[42] J.N. Reddy, C.D. Chin, THERMOMECHANICAL ANALYSIS OF FUNCTIONALLY GRADED CYLINDERS AND PLATES, Journal of Thermal Stresses 21 (1998) 593–626. https://doi.org/10.1080/01495739808956165.

[43] A.M. Zenkour, M. Sobhy, Thermal buckling of various types of FGM sandwich plates, Composite Structures 93 (2010) 93–102. https://doi.org/10.1016/j.compstruct.2010.06.012.

[44] J.N. Reddy, Analysis of functionally graded plates, Int. J. Numer. Meth. Engng. 47 (2000) 663–684. https://doi.org/10.1002/(SICI)1097-0207(20000110/30)47:1/3%253C663::AID-NME787%253E3.0.CO;2-8.

[45] A. Chedad, N. Elmeiche, S. Hamzi, H. Abbad, Effect of porosity on the thermal buckling of functionally graded material (FGM) sandwich plates under different boundary conditions, Mechanics Based Design of Structures and Machines 52 (2022) 1414–1436. https://doi.org/10.1080/15397734.2022.2148691.

[46] A.F. Radwan, Effects of non-linear hygrothermal conditions on the buckling of FG sandwich plates resting on elastic foundations using a hyperbolic shear deformation theory, Jnl of Sandwich Structures &; Materials 21 (2017)

289–319.
https://doi.org/10.1177/1099636217693557.